

# Calculation of the Pseudoscalar-Isoscalar Hadronic Current Correlation Functions of the Quark-Gluon Plasma

Bing He, Hu Li, C. M. Shakin,\* and Qing Sun

*Department of Physics and Center for Nuclear Theory*

*Brooklyn College of the City University of New York*

*Brooklyn, New York 11210*

(Dated: October, 2002)

## Abstract

We report the results of calculations of pseudoscalar-isoscalar hadronic current correlators using the Nambu–Jona-Lasinio model and the real-time finite-temperature formalism. (This work represents a continuation of results reported previously for other current correlators.) Results are presented for the temperatures range  $1.2 \leq T/T_c \leq 6.0$ , where  $T_c$  is the temperature of the confinement-deconfinement transition, which we take to be  $T_c = 170$  MeV. Some resonant features are seen in our calculations. In order to understand the origin of these resonances, we have performed relativistic random phase approximation (RPA) calculations of the temperature-dependent spectrum of the  $\eta$  mesons for  $T < T_c$ . For the RPA calculations, use is made of a simple model in which we introduce temperature-dependent constituent quark masses calculated in a mean-field approximation and a temperature-dependent confining interaction whose form is motivated by recent studies made using lattice simulations of QCD with dynamical quarks. We also introduce temperature-dependent coupling constants in our generalized NJL model. Our motivation in the latter case is the simulation of the approach to a weakly interacting system at high temperatures and the avoidance of “ $\eta$  condensates” which would indicate instability of the ground state of the model. We present some evidence that supports our use of temperature-dependent coupling constants for the NJL model. We suggest that our results may be of interest to researchers who use lattice simulations of QCD to obtain temperature dependent spectral functions for various hadronic current correlation functions.

PACS numbers: 12.39.Fe, 12.38.Aw, 14.65.Bt

---

\*email:casbc@cunyvm.cuny.edu

## I. INTRODUCTION

Recently we have seen a good deal of interest in the calculation of hadronic current correlation functions at finite temperature using lattice simulations of QCD [1-5]. The procedure involves the calculation of the correlation function in Euclidean space and the application of a generalized Laplace transform to obtain the spectral functions. Various temperature-dependent resonant structures are found in the spectral functions. It is of interest to obtain further understanding of the nature of these resonances using chiral Lagrangian models, such as that of the Nambu–Jona-Lasinio (NJL) model [6], that are successful in reproducing some of the low-energy properties of QCD. We have made some calculations of spectral functions making use of a generalized Nambu–Jona-Lasinio model [7]. In that work we studied correlators for currents with the quantum numbers of the  $a_0$ ,  $f_0$ ,  $\pi$ , and  $\rho$  mesons. In the present work we extend our study to the pseudoscalar-isoscalar correlators. In this case the correlators are calculated in terms of excitations that have the quantum numbers of the  $\eta$  mesons. One of our goals in the present study is to relate the pseudoscalar-isoscalar spectral functions to the properties of the  $\eta$  mesons at finite temperature. The temperature dependence of the spectrum of the eta mesons is obtained using our generalized NJL model which includes a covariant model of confinement [8-13]. At zero temperature our model provides an excellent fit to the properties of the  $\eta(547)$ ,  $\eta'(958)$  mesons and their radial excitations [12]. (The model gives quite satisfactory results for the decay constants and mixing angles of the  $\eta$  and  $\eta'$  mesons.) In order to obtain the spectrum of the eta mesons at finite temperature, we make some assumptions which lead to relatively simple calculations. For example, we use temperature-dependent mass values for the constituent quarks obtained in a mean-field analysis and also introduce a temperature-dependent confining interaction that is motivated by some recent results obtained in lattice simulations of QCD with dynamical quarks. In addition, we have introduced a temperature dependence of the coupling constants of the NJL model. Our original motivation for introducing that temperature dependence was to model the various physical mechanisms that work against the development of pion condensation [14]. However, in the present work we argue that, if the NJL model is to be used at high temperatures, such temperature dependence is needed to avoid results that are inconsistent with what is known about QCD thermodynamics. For our studies we have introduced coupling constants  $G(T) = G(0)[1 - 0.17T/T_c]$ , where  $T_c$  is the temperature

of the confinement-deconfinement transition, which we take to be  $T_c = 170$  MeV. At that temperature the coupling constants are reduced by 17%. The coupling constants are equal to zero beyond  $T = 5.88 T_c$ . Thus, we see that in this model the short-range interaction is present in the range  $0 \leq T \leq 5.88 T_c$ , while the confining interaction is taken to vanish for  $T \geq 1.2 T_c$ . That feature of the model is also consistent with what is known concerning QCD thermodynamics.

Ideally, it would be preferable if we could calculate the temperature-dependent spectrum of the  $\eta$  mesons, including the radial excitations, in the imaginary-time Matsubara formalism or in the real-time finite-temperature formalism [15, 16]. That is a formidable task which is beyond the scope of the present work, but might be considered at some future time. (On the whole, there are some unresolved questions concerning the use of the field-theoretic finite-temperature theory in the confined phase of QCD which are not present when considering the deconfined phase.) In those cases in which our results may be compared to those of the Matsubara formalism we find general agreement [17]. However, we need to assume for the present work that, with the use of temperature-dependent constituent quark mass values, a temperature-dependent confining interaction and temperature-dependent coupling constants, we have introduced the most important features that influence the  $\eta$  spectrum for  $T < T_c$ .

The organization of our work is as follows. In Section II we discuss the calculation of polarization functions of the NJL model at finite temperature. In Section III we describe the calculation of the pseudoscalar-isoscalar hadronic current correlation functions and present various results of our numerical computations. Since the use of temperature-dependent coupling constants is an unusual feature of our model, we provide some justification for the use of such coupling constants in Section IV. In Section V we introduce the Lagrangian of our model that is used for our RPA calculations. We make reference to the RPA equations that were used to calculate the properties of the  $\eta$  mesons at  $T = 0$  in earlier work and describe the motivation for the introduction of a temperature-dependent confining interaction. We present some results of our numerical calculations and relate the results of our RPA calculations for  $T < T_c$  to the results obtained for the correlation functions for  $T > T_c$ . Finally, Section VI contains some further discussion and conclusions.

## II. POLARIZATION FUNCTIONS AT FINITE TEMPERATURE

In an earlier work we carried out a Euclidean-space calculation of the up, down, and strange constituent quark masses taking into account the 't Hooft interaction and our confining interaction [18]. The 't Hooft interaction plays only a minor role, but does provide coupling of the equations for the various constituent masses. If we neglect the confining interaction and the 't Hooft interaction in the mean field calculation of the constituent masses, we can compensate for their absence by making a modest change in the value of  $G_S$ , the coupling constant of the NJL model. For the calculations of this work we calculate the quark masses using the formalism presented in the Klevansky review [19]. (Note that our value of  $G_S$  is twice the value of  $G$  used in that review.) The relevant equation is Eq. (5.38) of Ref. [19]. Here, we put  $\mu = 0$  and write

$$m(T) = m^0 + 4GN_c \frac{m(T)}{\pi^2} \int_0^\Lambda dp \frac{p^2}{E_p} \tanh\left(\frac{1}{2}\beta E_p\right), \quad (2.1)$$

where  $\Lambda = 0.631$  GeV is a cutoff for the momentum integral,  $\beta = 1/T$  and  $E_p = [\vec{p}^2 + m^2(T)]^{1/2}$ . In our calculations we replace  $G$  by  $G_S(T)/2$  and solve the equation

$$m(T) = m^0 + 2G_S(T)N_c \frac{m(T)}{\pi^2} \int_0^\Lambda dp \frac{p^2}{E_p} \tanh\left(\frac{1}{2}\beta E_p\right), \quad (2.2)$$

with  $G_S(T) = 11.38[1 - 0.17 T/T_c]$  GeV,  $m_u^0 = 0.0055$  GeV and  $m_s^0 = 0.130$  GeV. Thus, we see that  $G_S(T)$  is reduced from the value  $G_S(0)$  by 17% when  $T = T_c$ . The results obtained in this manner for  $m_u(T)$  and  $m_s(T)$  are shown in Fig. 1. Here, the temperature dependence we have introduced for  $G_S(T)$  serves to provide a somewhat more rapid restoration of chiral symmetry than that which is found for a constant value of  $G_S$ . That feature and the temperature dependence of the confining potential leads to the deconfinement of the light mesons considered here at  $T \geq T_c$ .

For the calculation of polarization functions for  $T > 1.2 T_c$  we may neglect the confining interaction. However, we include temperature-dependent quark mass values in our calculations. The basic polarization functions that are calculated in the NJL model are shown in Fig. 2. We will consider calculations of such functions in the frame where  $\vec{P} = 0$ . In our earlier work, calculations were made after a confinement vertex was included. That vertex is represented by the filled triangular region in Fig. 2. However, we here consider calculations for  $T \geq 1.2 T_c$  where confinement may be neglected.

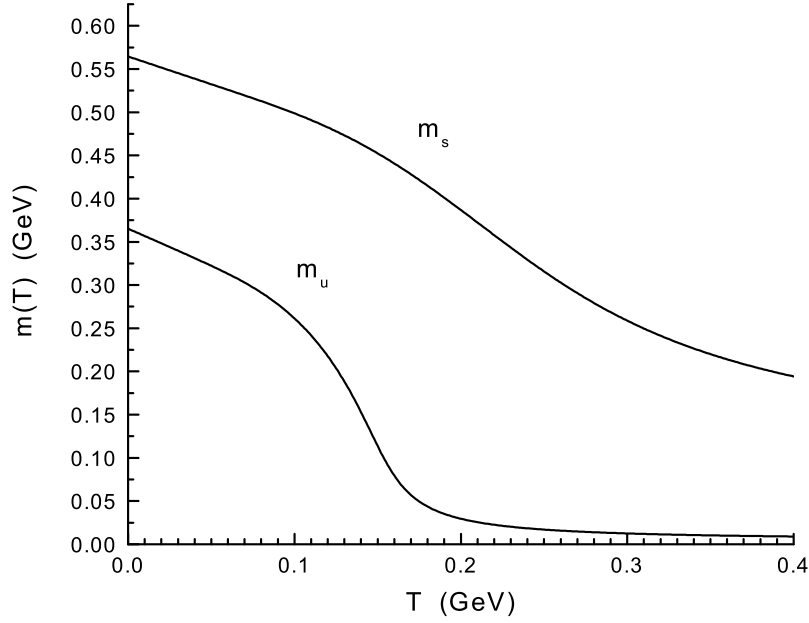


FIG. 1: Temperature dependent constituent mass values,  $m_u(T)$  and  $m_s(T)$ , calculated using Eq. (2.2) are shown. Here  $m_u^0 = 0.0055$  GeV,  $m_s^0 = 0.130$  GeV, and  $G(T) = 5.691[1 - 0.17(T/T_c)]$ , if we use Klevansky's notation [19].

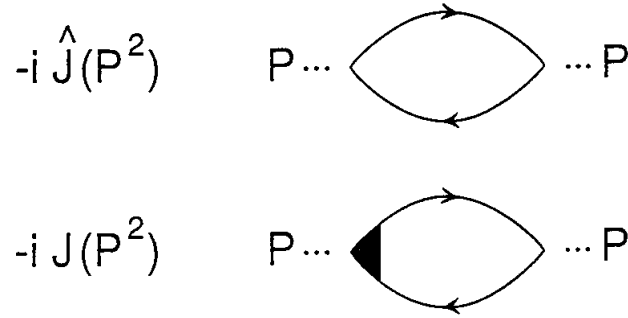


FIG. 2: The upper figure represents the basic polarization diagram of the NJL model in which the lines represent a constituent quark and a constituent antiquark. The lower figure shows a confinement vertex [filled triangular region] used in our earlier work. For the present work we neglect confinement for  $T \geq 1.2T_c$ , with  $T_c = 170$  MeV.

The procedure we adopt is based upon the real-time finite-temperature formalism, in which the imaginary part of the polarization function may be calculated. Then, the real part of the function is obtained using a dispersion relation. The result we need for this

work has been already given in the work of Kobes and Semenoff [20]. (In Ref. [20] the quark momentum in Fig. 2 is  $k$  and the antiquark momentum is  $k - P$ . We will adopt that notation in this section for ease of reference to the results presented in Ref. [20].) With reference to Eq. (5.4) of Ref. [20], we write the imaginary part of the scalar polarization function as

$$\begin{aligned} \text{Im } J^S(P^2, T) = & \frac{1}{2}(2N_c)\beta_S \epsilon(p^0) \int \frac{d^3k}{(2\pi)^3} e^{-\vec{k}^2/\alpha^2} \left( \frac{2\pi}{2E_1(k)2E_2(k)} \right) \\ & \{ (1 - n_1(k) - n_2(k))\delta(p^0 - E_1(k) - E_2(k)) \\ & - (n_1(k) - n_2(k))\delta(p^0 + E_1(k) - E_2(k)) \\ & - (n_2(k) - n_1(k))\delta(p^0 - E_1(k) + E_2(k)) \\ & - (1 - n_1(k) - n_2(k))\delta(p^0 + E_1(k) + E_2(k)) \} . \end{aligned} \quad (2.3)$$

Here,  $E_1(k) = [\vec{k}^2 + m_1^2(T)]^{1/2}$ . Relative to Eq. (5.4) of Ref. [20], we have changed the sign, removed a factor of  $g^2$  and have included a statistical factor of  $2N_c$ , where the factor of 2 arises from the flavor trace. In addition, we have included a Gaussian regulator,  $\exp[-\vec{k}^2/\alpha^2]$ , with  $\alpha = 0.605$  GeV, which is the same as that used in most of our applications of the NJL model in the calculation of meson properties [8-15]. We also note that

$$n_1(k) = \frac{1}{e^{\beta E_1(k)} + 1} , \quad (2.4)$$

and

$$n_2(k) = \frac{1}{e^{\beta E_2(k)} + 1} . \quad (2.5)$$

For the calculation of the imaginary part of the polarization function, we may put  $k^2 = m_1^2(T)$  and  $(k - P)^2 = m_2^2(T)$ , since in that calculation the quark and antiquark are on-mass-shell. We will first remark upon the calculation of scalar correlators. In that case, the factor  $\beta_S$  in Eq. (2.3) arises from a trace involving Dirac matrices, such that

$$\beta_S = -\text{Tr}[(\not{k} + m_1)(\not{k} - \not{P} + m_2)] \quad (2.6)$$

$$= 2P^2 - 2(m_1 + m_2)^2 , \quad (2.7)$$

where  $m_1$  and  $m_2$  depend upon temperature. In the frame where  $\vec{P} = 0$ , and in the case  $m_1 = m_2$ , we have  $\beta_S = 2P_0^2(1 - 4m^2/P_0^2)$ . For the scalar case, with  $m_1 = m_2$ , we find

$$\text{Im } J^S(P^2, T) = \frac{N_c P_0^2}{4\pi} \left( 1 - \frac{4m^2}{P_0^2} \right)^{3/2} e^{-\vec{k}^2/\alpha^2} [1 - 2n_1(k)] , \quad (2.8)$$

where

$$\vec{k}^2 = \frac{P_0^2}{4} - m^2(T). \quad (2.9)$$

We may evaluate Eq. (2.8) for  $m(T) = m_u(T) = m_d(T)$  and define  $\text{Im } J_u^S(P^2, T)$ . Then we put  $m(T) = m_s(T)$ , we define  $\text{Im } J_s^S(P^2, T)$ . These two functions are needed for a calculation of the scalar-isoscalar correlator. (Note that the factor of 2 arising from the flavor trace should be moved when we define the polarization function for a specific quark flavor.) The real parts of the functions  $J_u^S(P^2, T)$  and  $J_s^S(P^2, T)$  may be obtained using a dispersion relation, as noted earlier.

For pseudoscalar mesons, we replace  $\beta_S$  by

$$\beta_P = -\text{Tr}[i\gamma_5(\not{k} + m_1)i\gamma_5(\not{k} - \not{P} + m_2)] \quad (2.10)$$

$$= 2P^2 - 2(m_1 - m_2)^2, \quad (2.11)$$

which for  $m_1 = m_2$  is  $\beta_P = 2P_0^2$  in the frame where  $\vec{P} = 0$ . We find, for the  $\pi$  mesons,

$$\text{Im } J^P(P^2, T) = \frac{N_c P_0^2}{4\pi} \left(1 - \frac{4m(T)^2}{P_0^2}\right)^{1/2} e^{-\vec{k}^2/\alpha^2} [1 - 2n_1(k)], \quad (2.12)$$

where  $\vec{k}^2 = P_0^2/4 - m_u^2(T)$ , as above. Thus, we see that, relative to the scalar case, the phase space factor has an exponent of 1/2 corresponding to a  $s$ -wave amplitude, rather than the  $p$ -wave amplitude of scalar mesons. For the scalars, the exponent of the phase-space factor is 3/2, as seen in Eq. (2.8).

For a study of vector mesons we consider

$$\beta_{\mu\nu}^V = \text{Tr}[\gamma_\mu(\not{k} + m_1)\gamma_\nu(\not{k} - \not{P} + m_2)], \quad (2.13)$$

and calculate

$$g^{\mu\nu}\beta_{\mu\nu}^V = 4[P^2 - m_1^2 - m_2^2 + 4m_1m_2], \quad (2.14)$$

which, in the equal-mass case, is equal to  $4P_0^2 + 8m^2(T)$ , when  $m_1 = m_2$  and  $\vec{P} = 0$ . Note that for the elevated temperatures considered in this work  $m_u(T) = m_d(T)$  is quite small, so that  $4P_0^2 + 8m_u^2(T)$  can be approximated by  $4P_0^2$  when we consider the  $\rho$  meson. The generalization of these results for the study of the pseudoscalar-isoscalar correlators will be taken up in the next section.

### III. CALCULATION OF HADRONIC CURRENT CORRELATION FUNCTIONS

In this section we consider the calculation of temperature-dependent hadronic current correlation functions. The general form of the correlator is a transform of a time-ordered product of currents,

$$C(P^2, T) = i \int d^4x e^{ip \cdot x} \langle\langle T(j(x)j(0)) \rangle\rangle, \quad (3.1)$$

where the double bracket is a reminder that we are considering the finite temperature case.

For the study of pseudoscalar states, we may consider currents of the form  $j_{P,i}(x) = \bar{q}(x)i\gamma_5\lambda^i q(x)$ , where, in the case of the  $\pi$  mesons,  $i = 1, 2$ , and  $3$ . For the study of pseudoscalar-isoscalar mesons, we again introduce  $j_{P,i}(x) = \bar{q}(x)\lambda^i q(x)$ , but here  $i = 0$  for the flavor-singlet current and  $i = 8$  for the flavor-octet current.

In the case of the  $\pi$  mesons, the correlator may be expressed in terms of the basic vacuum polarization function of the NJL model,  $J_P(P^2, T)$  [19, 21, 22]. Thus,

$$C_\pi(P^2, T) = J_P(P^2, T) \frac{1}{1 - G_\pi(T)J_P(P^2, T)}, \quad (3.2)$$

where  $G_\pi(T)$  is the coupling constant appropriate for our study of the  $\pi$  mesons. We have found  $G_\pi(0) = 13.49 \text{ GeV}^{-2}$  by fitting the pion mass in a calculation made at  $T = 0$ , with  $m_u = m_d = 0.364 \text{ GeV}$  [14].

The calculation of the correlator for pseudoscalar-isoscalar states is more complex, since there are both flavor-singlet and flavor-octet states to consider. We may define polarization functions for  $u$ ,  $d$  and  $s$  quarks:  $J_u(P^2, T)$ ,  $J_d(P^2, T)$  and  $J_s(P^2, T)$ . (We recall that the factor of 2 arising from the flavor trace is not included when these functions are calculated.) In terms of these polarization functions we may then define

$$J_{00}(P^2, T) = \frac{2}{3}[J_u(P^2, T) + J_d(P^2, T) + J_s(P^2, T)], \quad (3.3)$$

$$J_{08}(P^2, T) = \frac{\sqrt{2}}{3}[J_u(P^2, T) + J_d(P^2, T) - 2J_s(P^2, T)], \quad (3.4)$$

and

$$J_{88}(P^2, T) = \frac{1}{3}[J_u(P^2, T) + J_d(P^2, T) + 4J_s(P^2, T)]. \quad (3.5)$$



We also introduce the matrices

$$J(P^2, T) = \begin{bmatrix} J_{00}(P^2, T) & J_{08}(P^2, T) \\ J_{80}(P^2, T) & J_{88}(P^2, T) \end{bmatrix}, \quad (3.6)$$

$$G(T) = \begin{bmatrix} G_{00}(T) & G_{08}(T) \\ G_{80}(T) & G_{88}(T) \end{bmatrix}, \quad (3.7)$$

and

$$C(P^2, T) = \begin{bmatrix} C_{00}(P^2, T) & C_{08}(P^2, T) \\ C_{80}(P^2, T) & C_{88}(P^2, T) \end{bmatrix}. \quad (3.8)$$

We then write the matrix relation

$$C(P^2, T) = J(P^2, T)[1 - G(T)J(P^2, T)]^{-1}. \quad (3.9)$$

For some purposes it may be useful to also define a  $t$  matrix

$$t(P^2, T) = [1 - G(T)J(P^2, T)]^{-1}G(T), \quad (3.10)$$

where  $t(P^2, T)$  has the structure shown in Eqs. (3.6)-(3.8). The same resonant structures are seen in both  $C(P^2, T)$  and  $t(P^2, T)$ .

Some of our results for the imaginary parts of the pseudoscalar-isoscalar correlators  $C_{00}(P^2)$ ,  $C_{88}(P^2)$  and  $C_{08}(P^2)$  are shown in Figs. 3, 4 and 5, respectively. In these figures the values are  $T/T_c = 1.2$  [solid line],  $T/T_c = 1.6$  [dashed line],  $T/T_c = 2.0$  [dotted line],  $T/T_c = 4.0$  [dashed-dotted line] and  $T/T_c = 6.0$  [dashed-(double)dotted line]. There is a large peak seen in Figs. 3-5 at about 775 MeV. It is worth noting that the state that evolves from the  $\eta'(958)$  with increasing temperature has a mass of about 750 MeV for  $T \simeq T_c$ . However, an analysis of the mixing angle for the state at 775 MeV shows that it is mainly an  $s\bar{s}$  state. Further work is needed to understand the relation between the bound-state spectrum for  $T < T_c$  and the resonant structures seen for  $T > T_c$ . We discuss the temperature dependence of the  $\eta$  spectrum in the Section V.

#### IV. TEMPERATURE-DEPENDENT COUPLING CONSTANTS OF THE NJL MODEL

Since the introduction of temperature-dependent coupling constants for the NJL model is a novel feature of our work, we provide arguments in this section to justify their introduction.

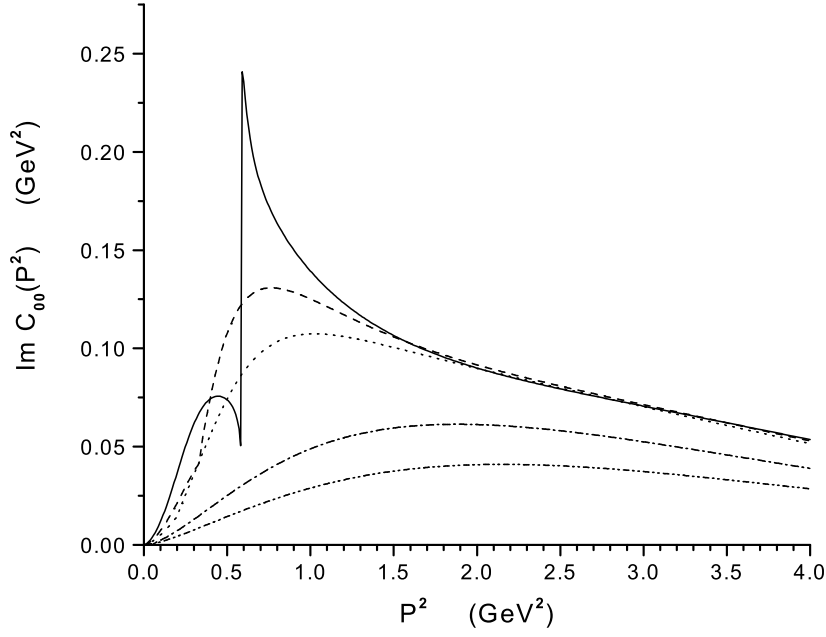


FIG. 3: The imaginary part of the pseudoscalar-isoscalar correlator  $C_{00}(P^2)$  is shown. Here,  $T/T_c = 1.2$  [solid line],  $1.6$  [dashed line],  $2.0$  [dotted line],  $4.0$  [dashed-dotted line] and  $6.0$  [dashed-(double)dotted line]. In this work we use  $G_{00} = 8.09 \text{ GeV}^{-2}$ ,  $G_{88} = 13.02 \text{ GeV}^{-2}$  and  $G_{08} = -0.4953 \text{ GeV}^{-2}$ .

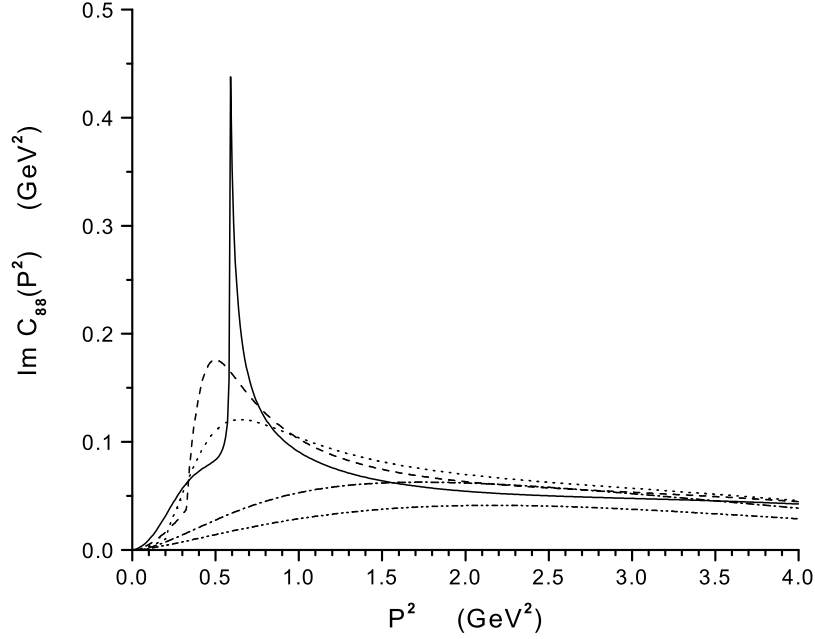


FIG. 4: The imaginary part of the correlator  $C_{88}(P^2)$  is shown. [See caption to Fig. 3.]

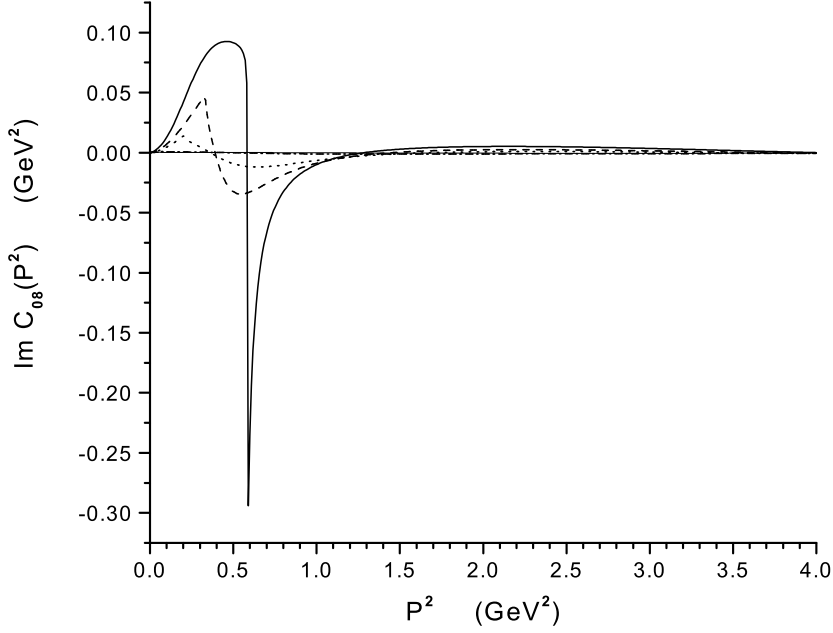


FIG. 5: The imaginary part of the correlator  $C_{08}(P^2)$  is shown. [See caption to Fig. 3.]

We make reference to Fig. 1.3 of Ref. [16]. That figure shows the behavior of the ratio  $\epsilon/T^4$  and  $3P/T^4$  for the pure gauge sector of QCD. Here  $\epsilon$  is the energy density and  $P$  is the pressure. Ideal gas behavior implies  $\epsilon = 3P$ . The values of  $\epsilon/T^4$  and  $3P/T^4$  are compared to the value  $\epsilon_{SB}/T^4 = 8\pi^2/15$  for an ideal gluon gas. It may be seen from the figure that at  $T = 3T_c$  there are still significant differences from the ideal gluon gas result. Deviations from ideal gas behavior become progressively smaller with increasing  $T/T_c$  and could be considered to be relatively unimportant for  $T/T_c > 5$ .

The use of our energy-dependent coupling constants is meant to be consistent with the approach to asymptotic freedom at high temperature. In order to understand this feature in our model, we can calculate the correlator with *constant* values of  $G_{00}$ ,  $G_{88}$  and  $G_{08}$  and with  $G_{00}(T) = G_{00}[1 - 0.17 T/T_c]$ , etc. (In this work we use  $G_{00} = 8.09 \text{ GeV}^{-2}$ ,  $G_{88} = 13.02 \text{ GeV}^{-2}$  and  $G_{08} = -0.4953 \text{ GeV}^{-2}$ .)

We now consider the values of  $\text{Im } C_{88}(P^2)$  for  $T/T_c = 4.0$ . In Fig. 6 we show the values of  $\text{Im } C_{88}(P^2)$  calculated in our model with temperature-dependent coupling constants as a dashed line. The dotted line shows the values of the correlator for  $G_{00} = G_{88} = G_{08} = 0$ , while the solid line shows the values when the coupling constants are kept at their values at  $T = 0$ . We see that we have some resonant behavior in the case the constants are temperature independent.

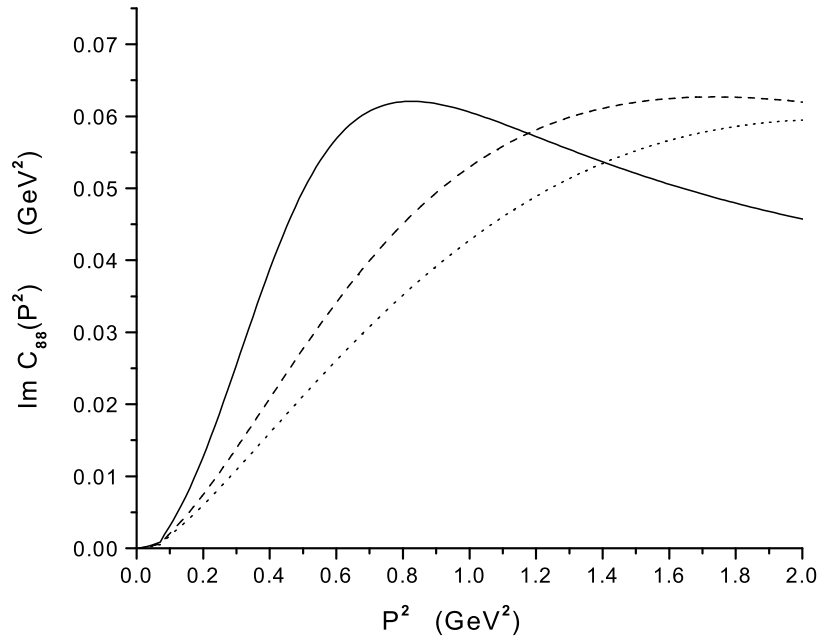


FIG. 6: The imaginary part of the correlator  $C_{88}(P^2)$  is shown for  $T/T_c = 4.0$ . The dashed line is the result for the temperature-dependent coupling constants of our model, while the solid line represents the results for coupling constants kept at their  $T = 0$  values. [See caption to Fig. 3.] The dotted line shows the values of the correlator when the coupling constants are set equal to zero.

In Fig. 7 we show similar results for  $T/T_c = 5.88$ . Here the temperature-dependent coupling constants are equal to zero, so that the lines corresponding to the dashed and dotted lines of Fig. 6 coincide. The solid line again shows some resonant behavior at a value of  $T/T_c$ , where we expect only very weak interactions associated with asymptotic freedom. We conclude that the model with constant values of the coupling constants yields unacceptable results, while our model, which has temperature-dependent coupling constants, behaves as one may expect, when the results of lattice simulations of QCD thermodynamics are taken into account.

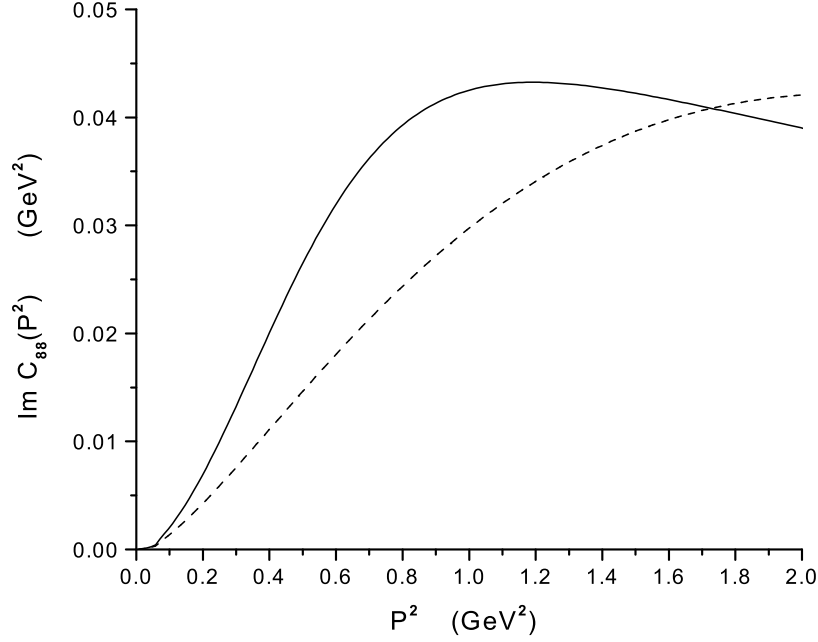


FIG. 7: The imaginary part of the correlator  $C_{88}(P^2)$  is shown for  $T/T_c = 5.88$ . [See caption to Fig. 6.] Here the dashed and dotted lines of Fig. 6 coincide.

## V. CALCULATION OF MESON PROPERTIES AT FINITE TEMPERATURE IN A GENERALIZED NJL MODEL WITH CONFINEMENT

It is useful to record the Lagrangian used in our calculations of meson properties

$$\begin{aligned}
\mathcal{L} = & \bar{q}(i\not{\partial} - m^0)q + \frac{G_S}{2} \sum_{i=0}^8 [(\bar{q}\lambda^i q)^2 + (\bar{q}i\gamma_5\lambda^i q)^2] \\
& - \frac{G_V}{2} \sum_{i=0}^8 [(\bar{q}\lambda^i\gamma_\mu q)^2 + (\bar{q}\lambda^i\gamma_5\gamma_\mu q)^2] \\
& + \frac{G_D}{2} \{\det[\bar{q}(1 + \gamma_5)q] + \det[\bar{q}(1 - \gamma_5)q]\} \\
& + \mathcal{L}_{conf},
\end{aligned} \tag{5.1}$$

Here,  $m^0$  is a current quark mass matrix,  $m^0 = \text{diag}(m_u^0, m_d^0, m_s^0)$ . The  $\lambda^i$  are the Gell-Mann (flavor) matrices,  $\lambda^0 = \sqrt{2/3}\mathbf{1}$  with  $\mathbf{1}$  being the unit matrix. The fourth term on the right-hand side of Eq. (5.1) is the 't Hooft interaction. Finally,  $\mathcal{L}_{conf}$  represents the model of confinement we have used in our work.

As noted earlier, we have recently reported results of our calculations of the temperature dependence of the spectra of various mesons [14]. These calculations were made using our

generalized NJL model which includes a covariant model of confinement. We have presented results for the  $\pi$ ,  $K$ ,  $a_0$ ,  $f_0$  and  $K_0^*$  mesons in Ref. [14]. The equations that we solve are of the form of relativistic random-phase-approximation equations. The derivation of these equations for pseudoscalar mesons is given in Ref. [13], where we discuss the equations for pionic, kaonic and eta mesons. The equations for the eta mesons are the most complicated, since we consider singlet-octet mixing as well as pseudoscalar-axial-vector mixing. In that case there are eight vertex functions to consider,  $\Gamma_{P,0}^{+-}$ ,  $\Gamma_{A,0}^{+-}$ ,  $\Gamma_{P,8}^{+-}$ ,  $\Gamma_{A,8}^{+-}$ ,  $\Gamma_{P,0}^{-+}$ ,  $\Gamma_{A,0}^{-+}$ ,  $\Gamma_{P,8}^{-+}$ ,  $\Gamma_{A,8}^{-+}$ , where  $P$  refers to the  $\gamma_5$  vertex and  $A$  refers to the  $\gamma_0\gamma_5$  vertex, which mixes with the  $\gamma_5$  vertex. Corresponding to the eight vertex functions one may define eight wave function amplitudes [13]. Since the RPA equations for the study of the eta meson are quite lengthy [13], we do not reproduce them here.

In the RPA equations we replace  $m_u$  and  $m_s$  by  $m_u(T)$  and  $m_s(T)$  of Fig. 1 and use the temperature-dependent coupling constants described earlier in this work. In addition to the temperature dependence of the coupling constants and constituent mass values, we also introduced a temperature-dependent confining potential, whose form was motivated by recent lattice simulations of QCD in which the temperature dependence of the confining interaction was calculated with dynamical quarks [23]. (See Fig. 8.) In order to include such effects, we modified the form of our confining interaction,  $V^C(r) = \kappa r \exp[-\mu r]$ , by replacing  $\mu$  by

$$\mu(T) = \frac{\mu_0}{\left[1 - 0.7 \left(\frac{T}{T_c}\right)^2\right]}, \quad (5.2)$$

with  $\mu_0 = 0.010$  GeV. The maximum value of  $V^C(r, T)$  is then

$$V_{max}^C(T) = \frac{\kappa}{\mu(T)e}, \quad (5.3)$$

$$= \frac{\kappa [1 - 0.7(T/T_c)^2]}{\mu_0 e}, \quad (5.4)$$

with  $r_{max} = 1/\mu(T)$ . To better represent the qualitative features of the results shown in Fig. 8, we use  $V^C(r, T) = \kappa r \exp[-\mu(T)r]$  for  $r \leq r_{max}$  and  $V^C(r, T) = V_{max}^C(T)$  for  $r > r_{max}$ . We also note that we use Lorentz-vector confinement and carry out all our calculations in momentum-space. (The value of  $\kappa$  used in our work is  $0.055 \text{ GeV}^2$ .) Values of  $V^C(r, T)$  are shown in Fig. 9.

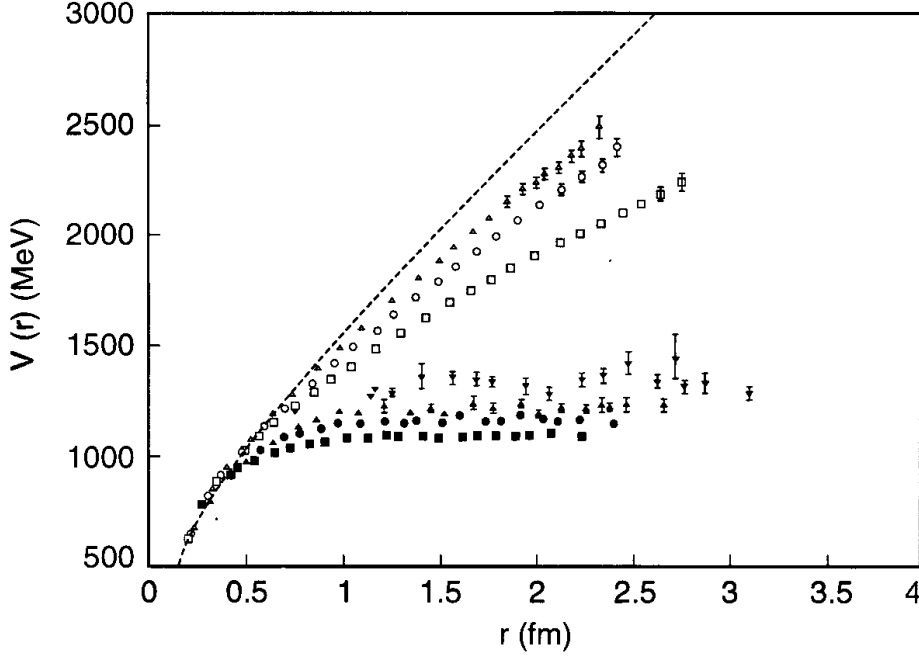


FIG. 8: A comparison of quenched (open symbols) and unquenched (filled symbols) results for the interquark potential at finite temperature [23]. The dotted line is the zero temperature quenched potential. Here, the symbols for  $T = 0.80T_c$  [open triangle],  $T = 0.88T_c$  [open circle], and  $T = 0.94T_c$  [open square], represent the quenched results. The results with dynamical fermions are given at  $T = 0.68T_c$  [solid downward-pointing triangle],  $T = 0.80T_c$  [solid upward-pointing triangle],  $T = 0.88T_c$  [solid circle], and  $T = 0.94T_c$  [solid square].

In Fig. 10 we show the results of our calculations of the temperature-dependent spectrum of the  $\eta$  mesons. We show the behavior of the  $\eta(547)$ ,  $\eta'(958)$  and seven states which represent radial excitations. The energies of the additional states found when diagonalizing the RPA Hamiltonian are represented by dots in the range  $0 \leq T/T_c \leq 0.6$ . We note that the masses of the nodeless states (the  $\eta$  and  $\eta'$ ) are fairly constant over a broad range of temperatures. That characteristic seems to be a feature of the behavior of pseudo-Goldstone bosons at finite temperature.

As the temperature is increased, fewer states are bound by the confining field which decreases in magnitude with increasing temperature. At  $T = T_c$  only the state that evolves from the  $\eta(547)$  is bound. That state disappears from the spectrum for  $T > T_c$ . We believe

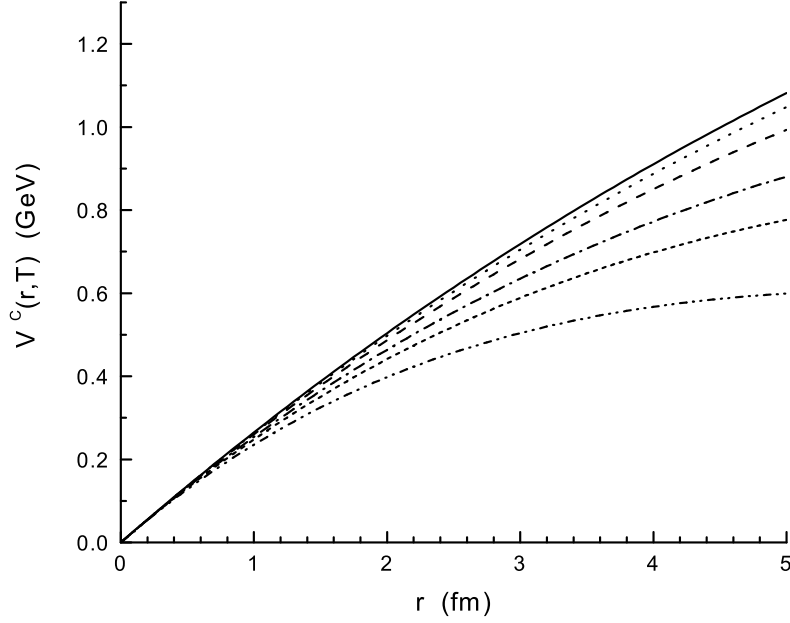


FIG. 9: The potential  $V^C(r, T)$  is shown for  $T/T_c = 0$  [solid line],  $T/T_c = 0.4$  [dotted line],  $T/T_c = 0.6$  [dashed line],  $T/T_c = 0.8$  [dashed-dotted line],  $T/T_c = 0.9$  [short dashes],  $T/T_c = 1.0$  [dashed-(double) dotted line]. Here,  $V^C(r, T) = \kappa r \exp[-\mu(T)r]$ , with  $\mu(T) = 0.01\text{GeV}/[1 - 0.7(T/T_c)^2]$  and  $\kappa = 0.055 \text{ GeV}^2$ .

that the crossing of levels seen at  $T/T_c = 0.9$  is due to the rapid decrease of  $m_u(T)$  relative to  $m_s(T)$  with increasing  $T/T_c$ . [See Fig. 1.] That feature could lead to a (predominately)  $n\bar{n}$  state with a node to have a lower energy than a (predominantly) nodeless  $s\bar{s}$  state.

## VI. DISCUSSION AND CONCLUSIONS

We believe is of interest to supplement lattice studies of hadronic current correlation functions with calculations made using chiral Lagrangian models of the type considered in this work. We have made some progress in exhibiting results for such correlators in Ref. [7] and in the present study. It might be of some interest to compare our results for our temperature-dependent RPA calculations with results obtained in the imaginary-time or real-time formalisms, if these formalisms could be modified so that calculations could be made in the confined phase of QCD. The study of radial excitations in these finite-temperature theories may be quite difficult since their study requires a model of confinement. It is also very difficult to obtain information concerning radial excitations, if an analytic



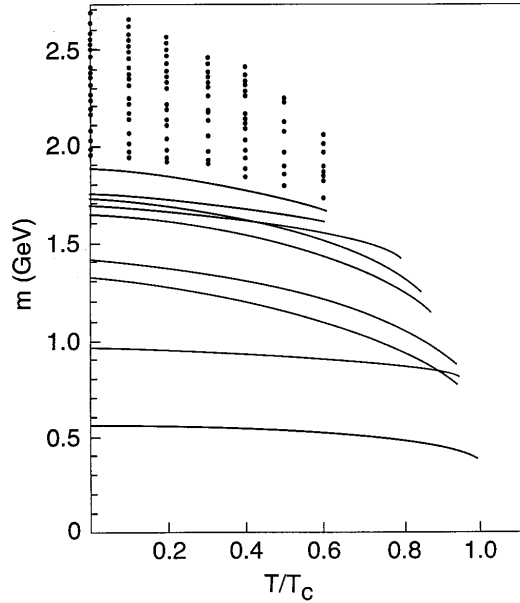


FIG. 10: The temperature-dependent spectrum of the  $\eta$  mesons is shown. For the most highly excited radial excitations we represent the mass values obtained by dots. There are no bound states for  $T > T_c$ .

continuation to real time is necessary.

One interesting feature of our analysis is the use of temperature-dependent coupling constants in the NJL model. In the present work, we have provided some justification for the introduction of such constants. Our work suggests that the coupling constants of the NJL model may also be density-dependent, since one expects that high density may play a similar role as high temperature, leading ultimately to a weakly interacting system at high density. We have introduced density-dependent coupling constants in Ref. [24] where we considered the confinement-deconfinement transition in the presence of matter. Since the study of matter at high density is a topic of active investigation [25-31], our suggestion of density-dependent coupling constants may have important consequences for such studies.

---

[1] M. Asakawa, T. Hatsuda and Y. Nakahara, hep-lat/0208059.

- [2] F. Karsch, S. Datta, E. Laermann, P. Petreczky, S. Stickan, and I. Wetzorke, hep-ph/0209028.
- [3] I. Wetzorke, F. Karsch, E. Laermann, P. Petreczky, and S. Stickan, Nucl. Phys. B (Proc. Suppl.) **106**, 510 (2002).
- [4] M. Asakawa, Y. Nakahara and T. Hatsuda, Prog. Part. Nucl. Phys. **46**, 459 (2001).
- [5] C. Allton, D. Blythe, and J. Clowser, Nucl. Phys. B (Proc. Suppl.) **109A**, 192 (2002).
- [6] Y. Nambu and G. Jona-Lasinio, Phys. Rev. **123**, 345 (1961); **124**, 246 (1961).
- [7] Hu Li and C. M. Shakin, hep-ph/0209258.
- [8] C. M. Shakin and Huangsheng Wang, Phys. Rev. D **63**, 014019 (2000).
- [9] L. S. Celenza, Huangsheng Wang, and C. M. Shakin, Phys. Rev. C **63**, 025209 (2001).
- [10] C. M. Shakin and Huangsheng Wang, Phys. Rev. D **63**, 074017 (2001).
- [11] C. M. Shakin and Huangsheng Wang, Phys. Rev. D **63**, 114007 (2001).
- [12] C. M. Shakin and Huangsheng Wang, Phys. Rev. D **64**, 094020 (2001).
- [13] C. M. Shakin and Huangsheng Wang, Phys. Rev. D **65**, 094003 (2002).
- [14] Hu Li and C. M. Shakin, Chiral symmetry restoration and deconfinement of light mesons at finite temperature, hep-ph/0209136.
- [15] J. I. Kapusta, *Finite Temperature Field Theory*, (Cambridge Univ. Press, Cambridge, U.K., 1989).
- [16] M. Le Bellac, *Thermal Field Theory*, (Cambridge Univ. Press, Cambridge, U.K., 1996).
- [17] P. Maris, C. D. Roberts, S. M. Schmidt, and P. C. Tandy, Phys. Rev. C **63**, 025202 (2001).
- [18] Bing He, Hu Li, Qing Sun, and C. M. Shakin, nucl-th/0203010.
- [19] S. P. Klevansky, Rev. Mod. Phys. **64**, 649 (1992). [See Eq. (5.38) of this reference.]
- [20] R. L. Kobes and G. W. Semenoff, Nucl. Phys. B **260**, 714 (1985).
- [21] T. Hatsuda and T. Kunihiro, Phys. Rep. **247**, 221 (1994).
- [22] U. Vogl and W. Weise, Prog. Part. Nucl. Phys. **27**, 195 (1991).
- [23] C. DeTar, O. Kaczmarek, F. Karsch, and E. Laermann, Phys. Rev. D **59**, 031501 (1998).
- [24] Hu Li and C. M. Shakin, Phys. Rev. D **66**, 074016 (2002).
- [25] For reviews, see K. Rajagopal and F. Wilcek, in *At the Frontier of Particle Physics/Handbook of QCD*, M. Shifman ed. (World Scientific, Singapore 2001); M. Alford, Annu. Rev. Nucl. Part. Sci. **51**, 131 (2001).
- [26] M. Alford, R. Rajagopal and F. Wilcek, Phys. Lett. B **422**, 247 (1998).
- [27] R. Rapp, T. Schäfer, E. V. Shuryak and M. Velkovsky, Phys. Rev. Lett. **81**, 53 (1998).

- [28] M. Alford, J. Berges and K. Rajagopal, Nucl. Phys. B **558**, 219 (1999).
- [29] J. Kundu and K. Rajagopal, Phys. Rev. D **65**, 094022 (2002).
- [30] S. Datta, F. Karsck, P. Petreczky and I. Wetzorke, hep-lat/0208012.
- [31] S. Digal, P. Petreczky, and H. Satz, Phys. Rev. D **64**, 094015 (2001).